https://doi.org/10.48048/tis.2024.8592

Structural Stability of Vacancy and Substitutional Defects in g-GaN: A First-Principles Study

Malika Fadlliyana[1], Nurul Fajariah[1], Pekik Nurwantoro[1], Harmon Prayogi[2], Diki Purnawati[3], Cristina Wulan Oktavina[1], Ari Dwi Nugraheni[1] and Sholihun Sholihun[1,*]

[1]Department of Physics, Faculty of Mathematics and Natural Sciences, Universitas Gadjah Mada, Yogyakarta 55281, Indonesia

[2]Department of Data Science, Faculty of Mathematics and Natural Sciences, Universitas Negeri Surabaya, Jawa Timur 60231, Indonesia

[3]Research Center for Electronics (PRE), National Research and Innovation Agency (BRIN), Jawa Barat 40135, Indonesia

([*]Corresponding author's e-mail: sholihun@ugm.ac.id)

Received: 20 June 2024, Revised: 29 July 2024, Accepted: 5 August 2024, Published: 20 October 2024

Abstract

Herein, the first-principles calculations of defected monolayer graphene-like gallium nitride (g-GaN) were elucidated. The optimized geometric revealed that the nearest-neighbor distances of N-N (between N atoms) and Ga-Ga (between Ga atoms) were narrowing in most configurations. Interestingly, the V_{Ga} has a similar atomic symmetry as the pure g-GaN, which is D_{3h}. Most defected configurations are degraded into C_{2V} symmetries, while the Stone-Wales configuration has the lowest symmetry of C_S. The formation energies of V_{Na} systems are lower, which implies better energetic stability. For the divacancies, the V_{Ga} system is more stable than the V_{Na} system. Moreover, the Stone-Wales configuration is energetically more stable than the interchange configuration. Furthermore, the reaction coordinates represent the geometric evolution of each defected system. The result revealed that the N-atoms are consistent with moving outward while the Ga-atoms move inward only for monovacancies and divacancies configurations. In contrast, the N-atoms move inward while the Ga-atoms move outward for substitutions, interchanges, and Stone-Wales configurations. We believe that this finding will be beneficial as the groundwork for future 2D g-GaN-based semiconductor devices.

Keywords: First-principles calculations, g-GaN, Defects, Symmetry, Stability

Introduction

Graphene possesses exceptional properties such as thermal conductivity and mechanical strength, which have led to the success of two-dimensional (2D) graphene-based device fabrications [1]. However,

low band gap energy is regarded as the major drawback of graphene (E_g ~ 0.3 - 0.4 eV), which limits its application [2,3]. Since then, numerous research studies have focused on 2D graphene-like materials, including silicene [4,5], germanene [5,6], and phosphorene [7]. Furthermore, materials beyond graphene, such as gallium nitride (GaN) [8,9], hexagonal boron nitride (h-BN) [10,11] and stannous carbonate (SnC) [12] have been widely explored. These materials are fascinating because of their wide band gap energies (E_g = 3 - 4 eV) [13,14]. Therefore, the research trends have been shifted to graphene-like structure exploration, mainly 2D GaN material.

The GaN has been regarded as a promising candidate for various semiconductor devices due to its wide band gap energy [13-16]. Over decades, GaN has been utilized as light-emitting diodes [17,18], laser diodes [19], power devices [20], devices [21], and detectors [22]. Aside from the wide band gap energy, GaN possesses excellent thermal and chemical stability [23], which is highly prospective for harsh environment applications such as high pressure and high temperature [24]. Other than that, GaN has also been widely utilized as a piezoelectric sensor owing to its sizeable piezoelectric constant [25].

Currently, extensive research has been dedicated to investigating the properties of the graphene-like GaN (g-GaN) material [8,26-28]. The g-GaN material is a 2D honeycomb-structured GaN having indirect wide band gap energy and low thermal conductivity [29-31]. Peng reported that the g-GaN material has superior mechanical properties to the g-BN counterpart [26]. Interestingly, the 2D g-GaN with Ga-vacancy defect is metallic, whereas the pristine 2D g-GaN is semiconductor. Moreover, the 2D g-GaN possesses strain-tunable magnetic properties, which is prospective for spintronic devices [8]. Furthermore, adding hydrogen atoms into g-GaN increases stability and enhances electronic properties [9]. In particular, the experimental studies of the 2D g-GaN have been demonstrated by Al Balushi *et al.* [27]. The 2D g-GaN has been successfully synthesized by utilizing graphene encapsulation. Consequently, the band gap energies of the 2D g-GaN have been modified to be around 4.18 - 5.00 eV [27,32]. Despite this, it was still unclear how various vacancy defects might affect the 2D g-GaN material.

This study evaluates various defect vacancies of the 2D g-GaN materials through density-functional theory (DFT) calculations. We simulated supercell g-GaN containing 72 atomic sites. Nine possible configurations, including vacancy and substitutional defect systems, were investigated. The vacancy systems consist of monovacancy by removing the Ga atom (V_{Ga}) or N atom (V_N), divacancy by removing Ga and N atoms as V_{GaN}, two atoms of Ga as V_{GaGa} and two atoms of N as V_{NN}. The substitutional systems consist of $S_{Ga\rightarrow N}$ (replacing the Ga atom instead of the N atom) and $S_{N\rightarrow Ga}$ (replacing the N atom instead of the Ga atom), interchange $I_{Ga\leftrightarrow N}$ (exchanging the position of the Ga and N atoms) and Stone-Wales configuration (rotating the Ga-N atoms by 90 °). Moreover, the equilibrium structural geometry, symmetry, formation energy, and the reaction coordinate are also studied. We expect our result to provide theoretical information about the defects in the 2D g-GaN, further contributing to developing optoelectronic devices.

Materials and methods

Herein, all calculations of the 2D g-GaN configurations are based on the first principles of density-functional theory (DFT) using the PHASE/0 code library [3,6,33]. We use ultra-soft pseudopotential and generalized gradient approximation (GGA) as functional exchange correlations [33]. We applied a 15 Å

vacuum in the z-direction, and the cut-off energy was set to 25 Ry. The unit cell consisting of 2 atoms (Ga-N) was optimized by calculating the total energy as a volume function. After that, the resulted-data were fitted by using the Birch-Murnaghan equation [10]:

After this, we enlarged the optimized unit cell by 6×6 times in the x- and y-directions, resulting in a supercell of 72 atoms (**Figure 1(a)**). The Brillouin zone (BZ) integration uses a 4×4×1 k-points Monkhorst-Pack grid. The monovacancies were modeled by removing single Ga- and N-atom of pristine GaN, as shown in **Figures 1(b) - 1(c)**, respectively. The divacancies were modeled by removing Ga-N, Ga-Ga, and N-N atoms, as illustrated in **Figures 1(d) - 1(f)**. The substitution configurations were created by replacing Ga-atom with N-atom and *vice versa* (**Figures 1(g) - 1(h)**, respectively). Moreover, the interchange configuration was obtained by exchanging the position of the Ga and N atoms (**Figure 1(i)**). Lastly, the Stone-Wales configuration was modeled by rotating the Ga-N atoms by 90 ° clockwise, as displayed in **Figure 1(j)**. Previous research shows SW defects formed by rotating 90 ° angles have better thermal stability than other rotation angles. The standard Stone-Wales (S-W) defect involves a 90 ° rotation, but under certain conditions, a rotation of less than 90 ° can occur due to local strains or environmental factors. However, these deviations are rare and less stable than the standard 90 ° rotation [34,35].

The supercell was relaxed, so the atomic forces were < 5.0×10^{-3} eV/Å. Then, we calculate the formation energies by using the following equation [10]:

$$E_f = E_d - (E_p - n\mu_{Ga} - m\mu_N) \quad (1)$$

where E_d , E_p, μ_{Ga} and μ_N are the total energy of the defective system, the total energy of pristine, the chemical potential of gallium, and the chemical potential of nitrogen. The n and m are the sum of vacancy of gallium and nitrogen. The chemical potential of isolated individual atoms in Eq. (1) is μ_{Ga} = −67.22 eV and μ_N = −266.23 eV. The distances between atoms were calculated using the following equation:

$$d_{ij} = \sqrt{(x_i - x_j)^2 + (y_i - y_j)^2 + (z_i - z_j)^2} \quad (2)$$

where $(x_i\, y_i\, z_i)$ and $(x_j\, y_j\, z_j)$ are the cartesian coordinates of atom i and atom j.

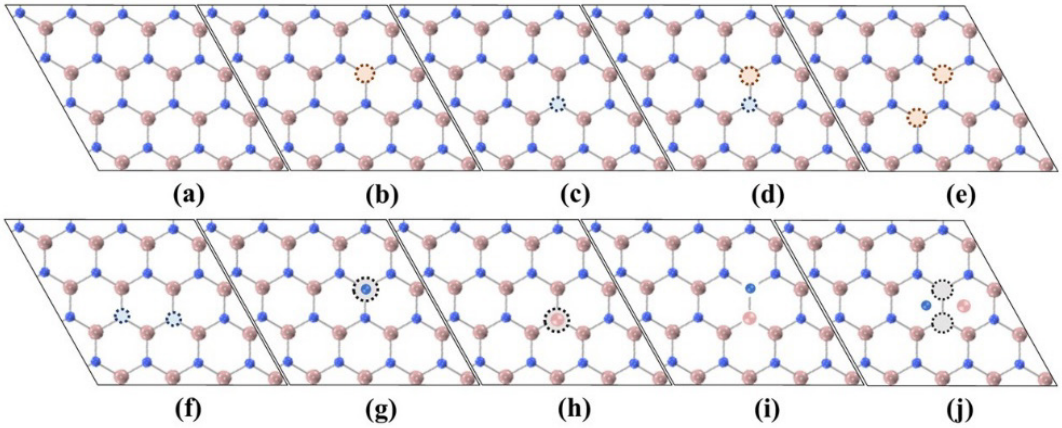

Figure 1 The structures of (a) monolayer GaN, (b) monovacancy of Ga, (c) monovacancy of N, (d) divacancies of Ga-N, (e) divacancies of Ga-Ga, (f) divacancies of N-N, (g) substitution of Ga with N, (h) substitution of N with Ga, (i) interchange of Ga-N and (j) Stone-Wales configurations.

Results and discussion

Optimized geometry

By utilizing the Birch-Murnaghan equation, the optimum lattice constant (α) of g-GaN was obtained at 3.318 Å, which is in ideal agreement with the literature [8,26,27,29,37]. The nearest-neighbor distance (Eq. (2)) of Ga-N atoms ($d_{\text{Ga-N}}$) in monolayer g-GaN was 1.87 Å, close to the previously reported work [26,29,36,37]. Whereas the d of N-N atoms ($d_{\text{N-N}}$) and Ga-Ga atoms ($d_{\text{Ga-Ga}}$) are 3.24 Å. Moreover, the d of defected g-GaN were also calculated and summarized in **Table 1**.

As a single Ga atom was removed, the $d_{\text{N-N}}$ were widened by 0.58 Å. Therefore, the $d_{\text{N-N}}$ of monovacancy Ga (V_{Ga}) was 3.82 Å, close to the previous work [37]. In the case of monovacancy N (V_{N}), the $d_{\text{Ga-Ga}}$ were varied at 3.20 - 3.46 Å. The $d_{\text{Ga-Ga}}$ in the x-direction were widened, while the $d_{\text{Ga-Ga}}$ in the y-direction was narrowed. In contrast, Gonzales *et al.* [37] reported that the $d_{\text{Ga-Ga}}$ of charged V_{N} were 3.00 - 3.11 Å.

The divacancy GaN (V_{GaN}) was created by simultaneously removing single atom Ga and single atom N. The result shows that the $d_{\text{Ga-Ga}}$ was narrowed (2.98 Å), while the $d_{\text{N-N}}$ was widened (3.67 Å) relative to the pure g-GaN. Likewise, the $d_{\text{N-N}}$ of divacancy Ga (V_{GaGa}) was also widened (3.72 Å). While the $d_{\text{Ga-Ga}}$ of divacancy N (V_{NN}) was narrowed by 0.24 to be 3.00 Å. Moreover, in the case of substitution Ga with N atom ($S_{\text{N}\rightarrow\text{Ga}}$), the $d_{\text{N-N}}$ are varied from 1.33 - 2.72 Å. On the contrary, the $d_{\text{Ga-Ga}}$ of $S_{\text{Ga}\rightarrow\text{N}}$ was narrowed by 0.96 Å concerning pure g-GaN. Interestingly, there is no significant change in the $d_{\text{Ga-N}}$ of interchanged Ga and N atoms. The $d_{\text{Ga-N}}$ remained the same as the pure g-GaN , which is 1.87 Å. Nevertheless, $d_{\text{Ga-Ga}}$ and $d_{\text{N-N}}$ were narrowed to b.32 and 1.52 Å, respectively. Similar behavior was also observed for the S-W configuration, where the $d_{\text{Ga-Ga}}$ and $d_{\text{N-N}}$ were narrowed (2.45 and 1.47 Å, respectively). Nevertheless, the $d_{\text{Ga-N}}$ were varied at 1.79 - 2.02 Å.

Table 1 Summarized lattice constants (α) and the nearest-neighbor distances (d) of defected g-GaN and the comparison to the references ([a][29], [b][38], [c][35], [d][27], [e][37] and [f][8]).

Structure	α (Å)	Reference (Å)	$d_{Ga\text{-}N}$ (Å)	$d_{Ga\text{-}Ga}$ (Å)	$d_{N\text{-}N}$ (Å)	Reference (Å)
g-GaN	3.318	3.170 - 3.209 [a-b, d-f]	1.87	3.24	3.24	1.85[a-c, e]
V_{Ga}	-	-	-	-	3.82	3.32[e]
V_N	-	-	-	3.20 - 3.46	-	3.00 - 3.11[e]
V_{GaN}	-	-	-	2.98	3.67	This work
V_{GaGa}	-	-	-	-	3.72	This work
V_{NN}	-	-	-	3.00	-	This work
$S_{Ga\rightarrow N}$	-	-	-	-	1.33 - 2.72	This work
$S_{N\rightarrow Ga}$	-	-	-	2.28	-	This work
$I_{Ga\leftrightarrow N}$	-	-	1.87	2.32	1.52	This work
S-W	-	-	1.79 - 2.02	2.45	1.47	This work

Furthermore, we also evaluate the symmetries of pure and defective g-GaN. It is well-known that the symmetry of honeycomb-structured graphene is D_{6h} [36]. Since the g-GaN is honeycomb-structured of diatomic material, the symmetry was lowered to be D_{3h}. Interestingly, as Ga monovacancy was created, the symmetry tends to remain as D_{3h}. In other words, the V_{Ga} didn't significantly affect the atomic symmetry. The symmetry continuously lowered as the N monovacancy was created. The symmetry of V_N is C_{2V}. Interestingly, the symmetry was consistent at C_{2V} for divacancy ($V_{GaN,}$ V_{GaGa} and V_{NN}), substitution ($S_{Ga\rightarrow N}$ and $S_{N\rightarrow Ga}$) and interchange ($I_{Ga\leftrightarrow N}$) configurations. In contrast, the S-W configuration has the lowest symmetry of C_S. The symmetries of all configurations are summarized in **Table 2**.

Formation energy

The formation energy (E_f) was calculated using Eq. (1). The E_f provide information on the atomic stability of the system. The lowest the E_f, the better the stability. Zhao *et al.* [4] reported that the E_f of the bulk GaN is 8.4 eV, and the E_f of the V_{Ga} is 7.67 eV. Herein, our calculation revealed that the E_f of the V_{Ga} of g-GaN was 8.21 eV, which is close to the reference. A super stability was observed for V_N where the E_f is 4.43 eV lower than the V_{Ga}. The E_f of V_N is 3.78 eV, as summarized in **Table 2**. A similar result was also reported by Gonzales *et al.* [37], where E_f of the V_{Ga} is higher than the V_N. In other words, the V_N has better stability than the V_{Ga}.

Furthermore, the configurations have symmetries of D_{3h}, C_{2v} and $C_{s,}$ as shown in **Table 2**. The D_{3h} symmetry has symmetry elements of C_3, C_2, S_6 and σ_d, while C_{2V} symmetry has symmetry elements of C_2, σ_{xz} and σ_{yz}. The configuration with the symmetry element of C_3 has a rotation by $\frac{\pi}{3}$. Therefore, the monovacancy belongs to D_{3h} symmetry in V_{Ga} and C_{2V} symmetry in V_N. The divacancy configurations have a symmetry of $C_{2V.}$ Like the divacancy, the substitution ($S_{Ga\rightarrow N}$ and $S_{N\rightarrow Ga}$) and interchange ($I_{Ga\leftrightarrow N}$) configurations have C_{2V} symmetries. Then, the Stone-Wales configuration has Cs symmetry (rotation by 2π and reflection σ_h).

In the case of the divacancies g-GaN, the E_f of $V_{GaN,}$ $V_{GaGa,}$ and V_{NN} are 14.85, 7.08, and 7.50, consecutively. The divacancies Ga and N are more stable than the divacancy GaN. The atomic nearest-neighbor distances of this system also reflected this behavior. Moreover, in the case of substitutions g-GaN, the E_f of $S_{Ga\rightarrow N}$ is 7.09 eV, while the E_f of $S_{N\rightarrow Ga}$ is −2.70 eV. The $S_{Ga\rightarrow N}$ configuration creates an N-rich system, while the $S_{N\rightarrow Ga}$ creates a Ga-rich system. The fact that the E_f of $S_{N\rightarrow Ga}$ is lower than the $S_{Ga\rightarrow N}$, it has been proven that the Ga-rich system exhibits better energetic stability, as mentioned above.

Table 1 Summarized symmetries and formation energies of defected g-GaN and the comparison to the references [a][36] and [b][37].

Structure	Symmetry	E_f (eV)	Reference (eV)
V_{Ga}	D_{3h}	8.21	7.67 - 7.82[a,b]
V_N	C_{2V}	3.78	2.62[b]
V_{GaN}	C_{2V}	14.85	This work
V_{GaGa}	C_{2V}	7.08	This work
V_{NN}	C_{2V}	7.50	This work
$S_{Ga\rightarrow N}$	C_{2V}	7.09	This work
$S_{N\rightarrow Ga}$	C_{2V}	-2.70	This work
$I_{Ga\leftrightarrow N}$	C_{2V}	13.62	This work
S-W	C_S	4.85	This work

Furthermore, the E_f of interchange configuration ($I_{Ga\leftrightarrow N}$) is 13.62 eV, higher than the bulk g-GaN (8.4 eV). This is likely due to the bond changing, which further restrained the system from reaching stability. On the other hand, the E_f of the S-W configuration is relatively low at 4.85 eV.

Geometric evolution

We evaluate the reaction coordinate of pure and defected g-GaN to elucidate the geometric changes from initial to final geometry. Herein, we observed 3 evolution states: Initial, transition, and final. The initial state of each system corresponds to the pure g-GaN system. As the defects were introduced, the systems started to enter their transition state by rearranging and relaxating atoms to reach their stable state. Ultimately, the final state represents the final atomic coordinates where the stability was successfully achieved.

Figure 2 shows the reaction coordinate of V_{Ga} where an outward relaxation occurred and further widened the system. Unlike in the V_{Ga} where the nearest-neighbor distances are uniform, the nearest-neighbor distances of V_N are non-uniform (**Figure 3**). In the case of V_N, atoms in the x-direction experience outward relaxation. Meanwhile, atoms in the y-direction experience inward relaxation. Hence, the final coordinates show non-uniform nearest-neighbor atomic distances, as shown in **Figure 3**.

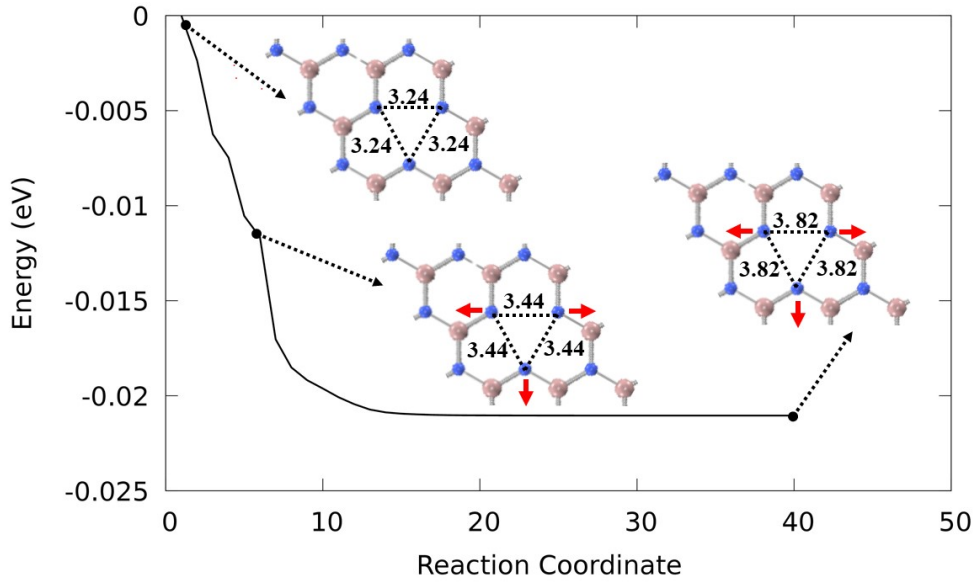

Figure 2 Reaction coordinate of the V_{Ga} configuration, representing the geometry optimization process from initial to final configuration.

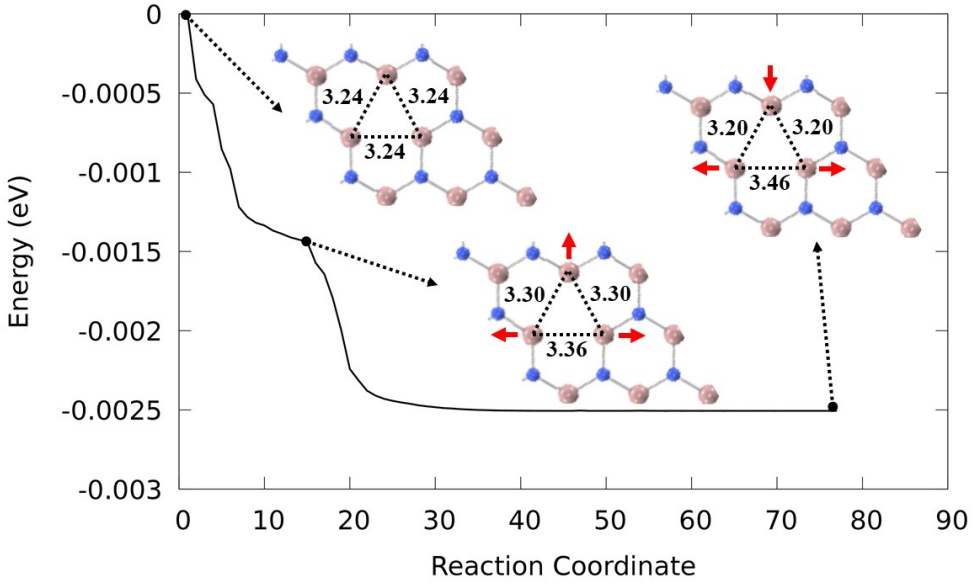

Figure 3 Reaction coordinate of the V_N configuration, representing the geometry optimization process from initial to final configuration.

In the case of divacancies, the V_{GaN} experiences both outward and inward relaxation. The outward relaxation occurred in the N-atoms, while the inward relaxation occurred in the Ga-atoms (**Figure 4**). Consistent with the V_{GaN}, N-atoms in the V_{GaGa} are experiencing outward relaxation (**Figure 5**). Whereas Ga-atoms in the V_{NN} moved oppositely (**Figure 6**). Concerning the monovacancies and divacancies g-GaN, it can be inferred that the Ga-Ga bonds tend to narrow the system, which leads to better energetic stability, as mentioned in the previous section. On the contrary, the N-N bonds tend to widen the system by relaxing

the system in the outward direction. Nonetheless, this behavior significantly degrades the energetic stability of the system.

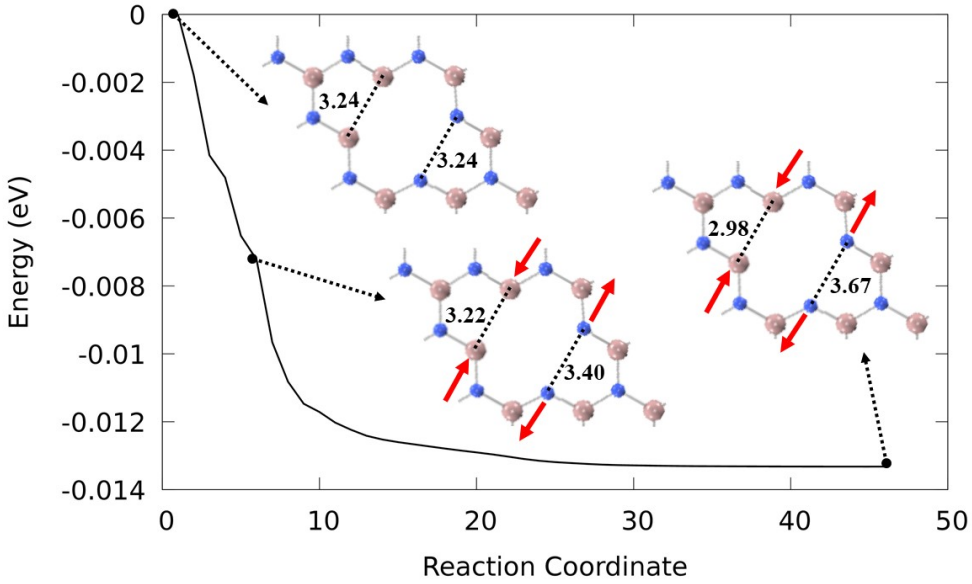

Figure 4 Reaction coordinate of the V_{GaN} configuration, representing the geometry optimization process from initial to final configuration.

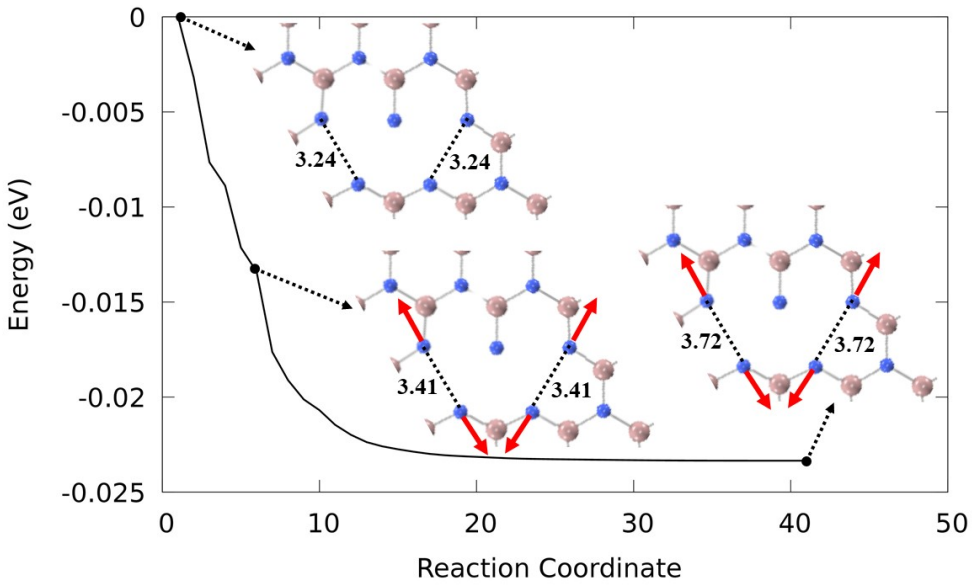

Figure 5 Reaction coordinate of the V_{GaGa} configuration, representing the geometry optimization process from initial to final configuration.

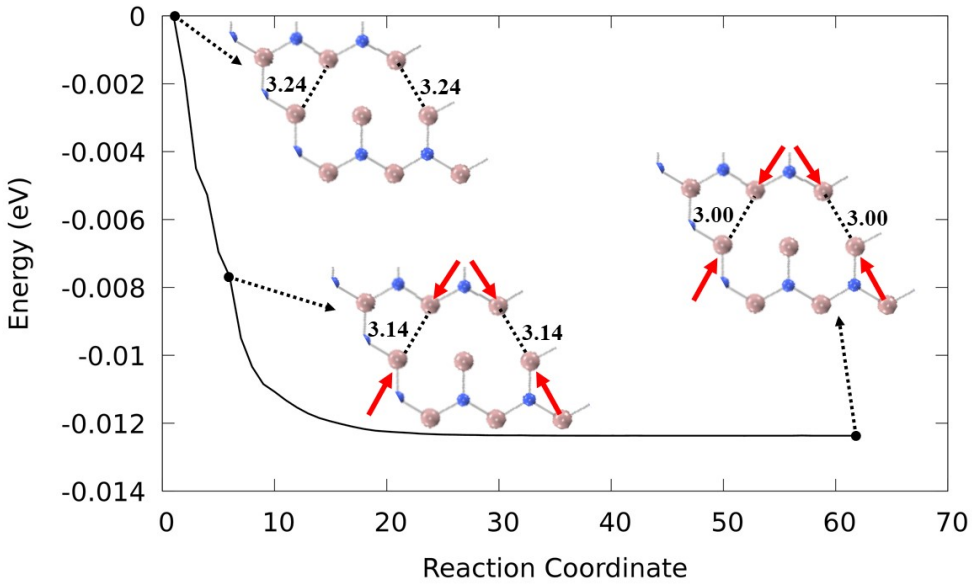

Figure 6 Reaction coordinate of the V_{NN} configuration, representing the geometry optimization process from initial to final configuration.

For the substitution configurations, the vacancies of the gallium system, which is also referred to as the $S_{N\rightarrow Ga}$ configuration, tend to form uniform-nearest-neighbor distances (**Figure 8**). The $S_{N\rightarrow Ga}$ experience uniform-outward relaxation in x- and y-directions. While the vacancies of the nitride system ($S_{Ga\rightarrow N}$ configuration) experience both outward (y-direction) and inward (x-direction) relaxation (**Figure 7**). Furthermore, this behavior significantly affects the energetical stability of the Ga-rich system ($S_{N\rightarrow Ga}$), as mentioned in the previous section.

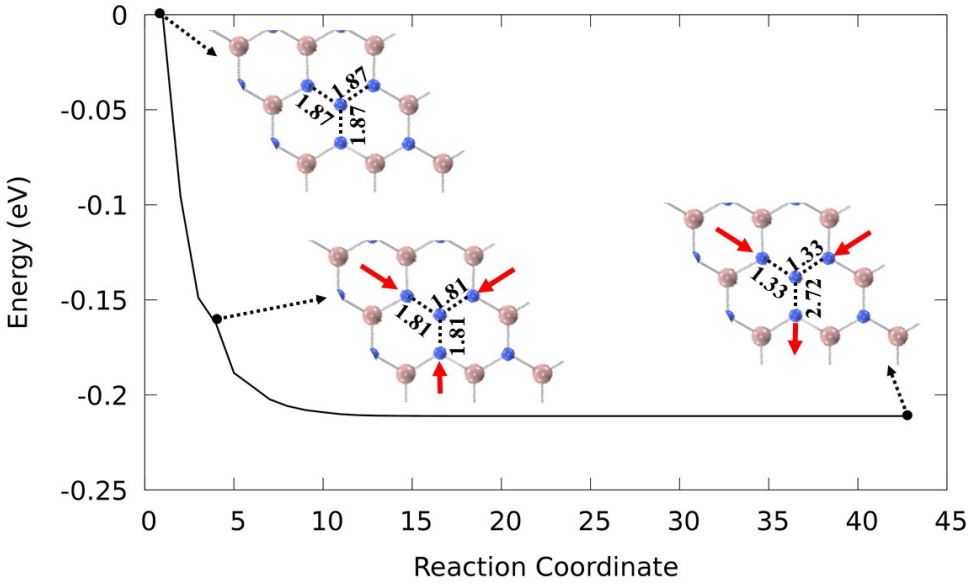

Figure 7 Reaction coordinate of the $S_{Ga\rightarrow N}$ configuration, representing the geometry optimization process from initial to final configuration.

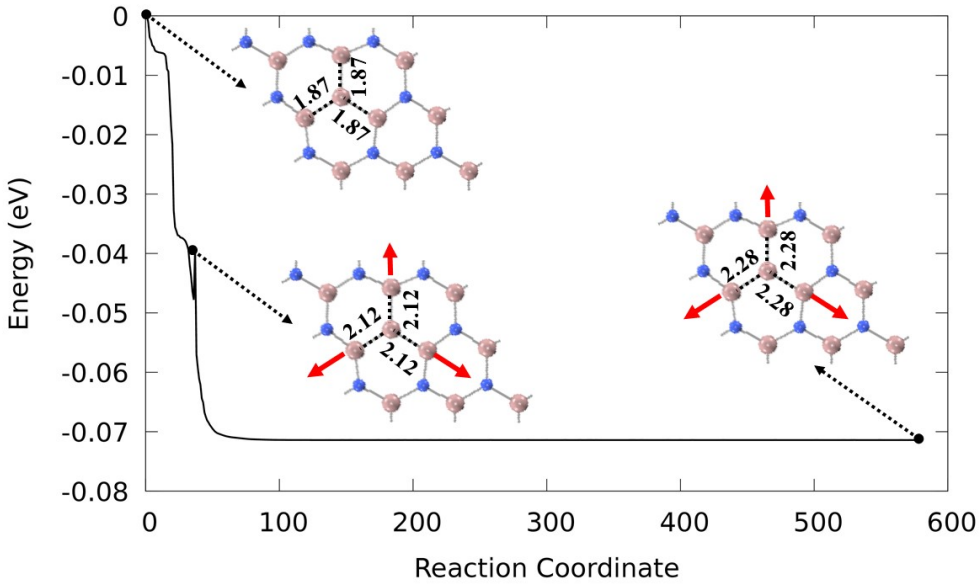

Figure 8 Reaction coordinate of the $S_{N\rightarrow Ga}$ configuration, representing the geometry optimization process from initial to final configuration.

Figure 9 shows the geometry evolution of interchange configuration. At the final state, the nearest-neighbor distances were varied from 1.52 to 2.32 Å. In other words, it experiences outward and inward relaxation in x- and y-directions. Moreover, the nearest-neighbor distances of the S-W configuration varied at 1.47 - 2.45 Å (**Figure 10**). Although both systems' nearest-neighbor distances vary, the relaxation patterns are consistent with the previous configurations. All N-N atoms are narrowing, while Ga-Ga atoms are widening.

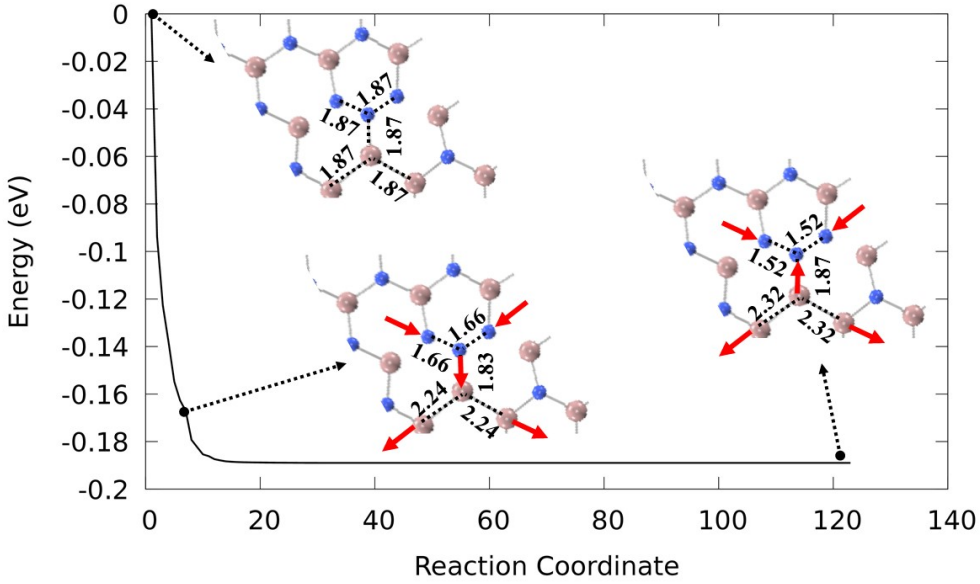

Figure 9 Reaction coordinate of the $I_{Ga\leftrightarrow N}$ configuration, representing the geometry optimization process from initial to final configuration.

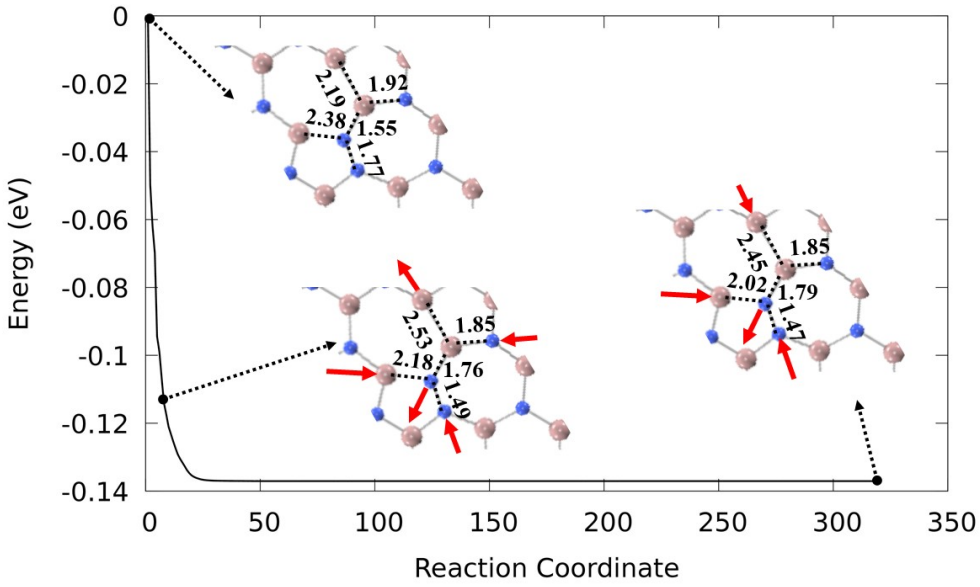

Figure 10 Reaction coordinate of the S-W configuration, representing the geometry optimization process from initial to final configuration.

Density of states

To investigate the electronic properties of g-GaN, we performed DOS calculations, shown in **Figure 11**. For the pristine g-GaN system, the DOS is shown in **Figure 11(a)**. Based on the figure, the pristine's gap energy is 2.09 eV. The DOS of monovacancy systems (V_{Ga} and V_N) are shown in **Figures 11(b) - 11(c)**. In the V_{Ga} system, a new peak state (~82 states/eV) appears near the Fermi level, decreasing the gap energy of 0.13 eV from the pristine one. Meanwhile, in the V_N system, the DOS shifts to the left, and the gap energy decreases to 0.12 eV.

Next, we calculate the DOS of the divacancy systems, shown in **Figures 11(d) - 11(f)**. In the $V_{Ga\text{-}Ga}$ system, the gap in the right of the Fermi level is 1.63 eV. However, since new states appeared across the Fermi level, the system has metallic behavior. The V_{NN} system produces new states near the Fermi level and leaves 1.65 eV on the left and 0.57 eV on the right of the Fermi level. The DOS of the V_{GaN} is like that of the V_{Ga} that new peak state (~60 states/eV) appears near the Fermi level, leaving a gap energy 1.76 eV. In the case of the substitutional defects, the $S_{Ga\rightarrow N}$ (**Figure 11(g)**) produces peak states, significantly decreasing gap energy to 0.56 eV. Like in the V_{NN}, the DOS of the $S_{N\rightarrow Ga}$ (**Figure 11(h)**) and S-W (**Figure 11(j)**) systems produces gaps of 0.56 and 1.27 eV on the left, and 0.89 and 1.06 eV on the right of the Fermi level, respectively. Some new states appear in the $I_{Ga\leftrightarrow N}$, leaving gap energies of 0.52 eV on the left and 0.34 eV on the right of the Fermi level, as shown in **Figure 11(i)**.

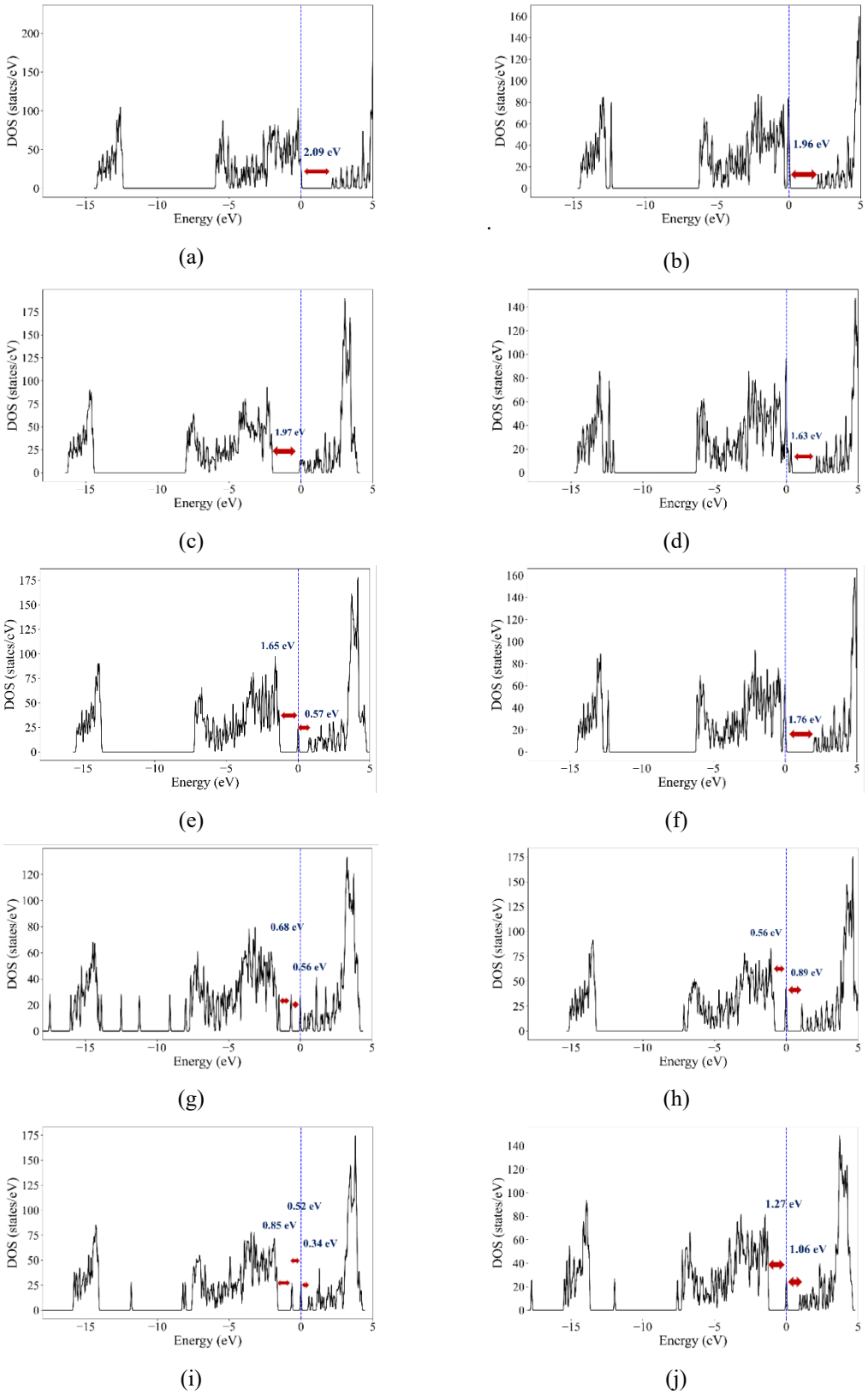

Figure 11 Density of states (a) pristine, (b) V_{Ga} configuration, (c) V_N configuration, (d) V_{GaGa} configuration (e), V_{NN} configuration, (f) V_{GaN} configuration, (g) $S_{Ga\rightarrow N}$ configuration, (h) $S_{N\rightarrow Ga}$ configuration, (i) interchange $I_{Ga\leftrightarrow N}$ configuration and (j) S-W configuration.

Conclusions

This study elucidates the behavior of defected g-GaN through the density-functional theory calculations. The optimized geometries, symmetries, formation energies and geometric evolutions were evaluated. In most cases, the $d_{\text{Ga-Ga}}$ and $d_{\text{N-N}}$ of defected g-GaN was narrowing as it reached the optimized geometry. Regarding atomic symmetries, the V_{Ga} is symmetric under $D_{3h,}$ like the pure g-GaN. After that, the symmetries tend to degrade into C_{2V} in most defective g-GaN configurations. In particular, the SW configuration has the lowest symmetry of C_S. Concerning the energetic stability, we evaluate the formation energies of each configuration. The minimum formation energy implies better energetic stability. The result revealed that the V_N system is more stable than the V_{Ga} system in the case of monovacancies and substitution configurations. Meanwhile, the V_{Ga} system seems more stable for the divacancies configurations. Furthermore, in the case of modified g-GaN atomic configurations, the Stone-Wales configuration is energetically more stable than the interchange configuration.

We also elucidate the geometric evolution by evaluating the reaction coordinates. We found that the N-atoms consistently move outward while the Ga-atoms move inward only for monovacancies and divacancies configurations. In contrast, the N-atoms move inward while the Ga-atoms move outward for substitutions, interchanges and Stone-Wales configurations. In addition, from the DOS calculations, the defects introduce new states, tending to decrease gap energies compared to the pristine system. This finding lays the groundwork for future g-GaN-based semiconductor electronic devices.

Acknowledgments

The computations use the ALELEON Supercomputer at EFISON Lisan Teknologi HQ, Indonesia.

References

[1] KS Novoselov, AK Geim, SV Morozov, D Jiang, MI Katsnelson, IV Grigorieva, SV Dubonos and AA Firsov. Two-dimensional gas of massless Dirac fermions in graphene. *Nature* 2005; **438**, 197-200.

[2] R Nandee, MA Chowdhury, A Shahid, N Hossain and M Rana. Band gap formation of 2D material in graphene: Prospect and challenges. *Results Eng.* 2022; **15**, 100474.

[3] S Sholihun, D Purnawati, JP Bermundo, H Prayogi, ZS Fatomi and S Hidayati. Novel two-dimensional square-structured diatomic group-IV materials: The first-principles prediction. *Phys. Scr.* 2023; **98**, 115903.

[4] S Li, Y Wu, Y Tu, Y Wang, T Jiang, W Liu and Y Zhao. Defects in silicene: Vacancy clusters, extended line defects and di-adatoms. *Sci. Rep.* 2015; **5**, 7881.

[5] M Ali, X Pi, Y Liu and D Yang. Electronic and magnetic properties of graphene, silicene and germanene with varying vacancy concentration. *AIP Adv.* 2017; **7**, 045308.

[6] DP Hastuti and P Nurwantoro. Stability study of germanene vacancies: The first-principles calculations. *Mater. Today Commun.* 2019; **19**, 459-63.

[7] T Hu and J Dong. Geometric and electronic structures of mono-and di-vacancies in phosphorene. *Nanotechnology* 2015; **26**, 065705.

[8] KH Yeoh, KH Chew, TL Yoon, R Rusi and DS Ong. Strain-tunable electronic and magnetic properties of two-dimensional gallium nitride with vacancy defects. *J. Appl. Phys.* 2020; **127**, 015305.

[9] DS Gomes, JM Pontes and S Azevedo. Structural and electronic properties of hydrogenated gallium nitride with vacancy and doping defects. *Appl. Phys. A* 2022; **128**, 1050.

[10] W Amalia and P Nurwantoro. Density-functional-theory calculations of structural and electronic propertis of vacancies in monolayer hexagonal boron nitride (h-BN). *Comput. Condes. Matter* 2019; **16**, e00354.

[11] AN Sosa, BJ Cid, IJ Hernández-Hernández and Á Miranda. Effects of substitutional doping and vacancy formation on the structural and electronic properties of silicene: A DFT study. *Mater. Lett.* 2022; **307**, 130993.

[12] S Majidi, A Achour, DP Rai, P Nayebi, S Solaymani, NB Nezafat and SM Elahi. Effect of point defects on the electronic density states of SnC nanosheets: First-principles calculations. *Results Phys.* 2017; **7**, 3209-15.

[13] D Bayerl, SM Islam, CM Jones, V Protasenko, D Jena and E Kioupakis. Deep ultraviolet emission from ultra-thin GaN/AlN heterostructures. *Appl. Phys. Lett.* 2016; **109**, 241102.

[14] N Sanders, D Bayerl, G Shi, KA Mengle and E Kioupakis. Electronic and optical properties of two-dimensional GaN from first principles. *Nano Lett.* 2017; **17**, 7345-9.

[15] V Singh, D Joung, L Zhai, S Das, SI Khondaker and S Seal. Graphene-based materials: Past, present and future. *Prog. Mater. Sci.* 2011; **56**, 1178-271.

[16] JH Ryou. *Gallium nitride (GaN) on sapphire substrates for visible LEDs. In*: JJ Huang, HC Kuo and SC Shen (Eds.). Nitride semiconductor Light-Emitting Diodes (LEDs): Materials, technologies and applications. Woodhead Publishing, Sawston, 2014, p. 66-98.

[17] T Mukai, S Nagahama, T Kozaki, M Sano, D Morita, T Yanamoto, M Yamamoto, K Akashi and S Masui. Current status and future prospects of GaN-based LEDs and LDs. *Phys. Status Solidi A* 2004; **201**, 2712-6.

[18] Y Taniyasu, M Kasu and T Makimoto. An aluminium nitride light-emitting diode with a wavelength of 210 nanometres. *Nature* 2006; **441**, 325-8.

[19] S Nakamura and MR Krames. History of gallium-nitride-based light-emiting diodes for illumination. *Proc. IEEE* 2013; **101**, 2211-20.

[20] T Ueda. Recent advances and future prospects on GaN-based power devices. *In*: Proceedings of the 2014 International Power Electronics Conference, Hiroshima, Japan. 2014.

[21] T Doi. Current status and future prospects of GaN substrates for green devices. *Sens. Mater.* 2013; **25**, 141-54.

[22] A Onen, D Kecik, E Durgun and S Ciraci. GaN: From three- to two-dimensional single-layer crystal and its multilayer van der Waals solids. *Phys. Rev. B* 2016; **93**, 085431.

[23] O Arbouche, B Belgoumène, B Soudini and M Driz. First principles study of the relative stability and the electronic properties of GaN. *Comput. Mater. Sci.* 2009; **47**, 432-8.

[24] FL Hsiao, TK Li, PC Chen, SC Wang, KW Lin, WL Lin, YP Tsai, WK Lin and BS Lin. Phase resonance and sensing application of an acoustic metamaterial based on a composite both-sides-open disk resonator arrays. *Sens. Actuators A Phys.* 2022; **339**, 113524.

[25] H Jiang, P Wan, J Yang, X Xu, W Li and X Li. Analysis of radiation defects in gallium nitride using deep level transient spectra and first principles methods. *Nucl. Instrum. Methods Phys. Res. Sect. B* 2022; **545**, 165120.

[26] Q Peng, C Liang, W Ji and S De. Mechanical properties of *g*-GaN: A first principles study. *Appl. Phys. A* 2013; **113**, 483-90.

[27] ZY Al Balushi, K Wang, RK Ghosh, RA Vilá, SM Eichfeld, JD Caldwell, X Qin, YC Lin, PA DeSario, G Stone, S Subramanian, DF Paul, RM Wallace, S Datta, JM Redwing and JA Robinson. Two-dimensional gallium nitride realized via graphene encapsulation. *Nat. Mater.* 2016; **15**, 1166-71.

[28] J Tian, L Liu and F Lu. Tuning the electronic and optical properties of two-dimensional GaN/AlGaN heterostructure by vacancy defect. *Appl. Surf. Sci.* 2022; **601**, 154269.

[29] H Şahin, S Cahangirov, M Topsakal, E Bekaroglu, E Akturk, RT Senger and S Ciraci. Monolayer honeycomb structures of group-IV elements and III-V binary compounds: First-principles calculations. *Phys. Rev. B* 2009; **80**, 155453.

[30] Q Chen, H Hu, X Chen and J Wang. Tailoring band gap in GaN sheet by chemical modification and electric field: *Ab initio* calculations. *Appl. Phys. Lett.* 2011; **98**, 053102.

[31] Z Qin, G Qin, X Zuo, Z Xiong and M Hu. Orbitally driven low thermal conductivity of monolayer gallium nitride (GaN) with planar honeycomb structure: A comparative study. *Nanoscale* 2017; **9**, 4295-309.

[32] W Wang, Y Li, Y Zheng, X Li, L Huang and G Li. Lattice structure and bandgap control of 2D GaN grown on graphene/Si heterostructures. *Small* 2019; **15**, 1802995.

[33] Y Dai, CX Yan, AY Li, Y Zhang and SH Han. Effects of hydrogen on electronic properties of doped diamond. *Carbon* 2005; **43**, 1009-14.

[34] MD Bhatt, H Kim and G Kim. Various defects in graphene: A review. *RSC Adv.* 2022; **12**, 21520-47.

[35] K Shen, BC Wang, Y Xiao and XF Wang. Stability of Stone-Wales defect in two-dimensional honeycomb crystals. *J. Phys. Condens. Matter* 2021; **33**, 335001.

[36] CN Brock, BB Baer and DG Walker. Low-valency gallium PAW for faster defect calculations in GaN using plane-wave DFT. *Comput. Mater. Sci.* 2020; **187**, 110106.

[37] R González, W López-Pérez, Á González-García, MG Moreno-Armenta and R González-Hernández. Vacancy-charged defects in two-dimensional GaN. *Appl. Surf. Sci.* 2018; **433**, 1049-55.

[38] X Wei, B Fragneaud, CA Marianetti and JW Kysar. Nonlinear elastic behavior of graphene: *Ab initio* calculations to continuum description. *Phys. Rev. B* 2009; **80**, 205407.